Aerosol Science and Technology, 39:17–29, 2005

ISSN: 0278-6826 print / 1521-7388 online
DOI: 10.1080/027868290901972

Towards Aerosol Light-Absorption Measurements with a 7-Wavelength Aethalometer: Evaluation with a Photoacoustic Instrument and 3-Wavelength Nephelometer

W. Patrick Arnott,[1] Khadeejeh Hamasha,[1] Hans Moosmüller,[1] Patrick J. Sheridan,[2] and John A. Ogren[2]
[1]*Desert Research Institute, Reno, Nevada, USA*
[2]*NOAA Climate Monitoring and Diagnostics Laboratory, Boulder, Colorado, USA*

Two extreme cases of aerosol optics from the Reno Aerosol Optics Experiment are used to develop a model-based calibration scheme for the 7-wavelength aethalometer. The cases include those of very white and very dark aerosol samples. The former allows for an assessment of the scattering offset associated with this filter-based method, with the wavelength-dependent scattering measured from a 3-wavelength nephelometer, and interpolated and extrapolated to the 7 wavelengths of the aethalometer. A photoacoustic instrument operating at 532 nm is used to evaluate the filter loading effect caused by aerosol light absorption. Multiple scattering theory is used to analytically obtain a filter-loading correction function. This theory shows that the exponential behavior of light absorption in the strong multiple scattering limit scales as the square root of the total absorption optical depth rather than linearly with optical depth as is commonly assumed with Beer's law. The multiple scattering model also provides a theoretical justification for subtracting a small fraction of aerosol light scattering away from measured apparent light absorption by the filter method. The model is tested against ambient measurements and is found to require coefficients that are situation specific. Several hypotheses are given for this specificity, and suggested methods for reducing it are discussed. Specific findings are as follows. Simultaneous aerosol light-scattering measurements are required for accurate interpretation of aethalometer data for high aerosol single-scattering albedo. Instantaneous errors of up to ±50% are possible for uncorrected data, depending on filter loading. The aethalometer overpredicts black carbon (BC) concentration on a fresh filter and underpredicts BC on a loaded filter. BC and photoacoustic light absorption can be tightly correlated if the data are averaged over the full range of filter loadings and the aerosol source is constant. Theory predicts that the Aethalometer response may be sensitive to filter face velocity, and hence flow rate, to the extent that particle penetration depth depends on face velocity.

Received 14 March 2004; accepted 22 October 2004.

We gratefully acknowledge encouragement and funding support from the NOAA Office of Global Programs, Aerosol–Climate Interactions Program, and the DOE Atmospheric Radiation Measurement Program. Photoacoustic instrument development was supported by the National Science Foundation and the Desert Research Institute. We acknowledge the assistance of John Walker and Mark Green, both from the Desert Research Institute, with the Las Vegas data.

Address correspondence to W. Patrick Arnott, Desert Research Institute, 2215 Raggio Parkway, Reno, NV 89512, USA. E-mail: pat@dri.edu

INTRODUCTION

Aerosol light-absorption measurements are important for health, climate, and visibility applications (Andreae 2001). The wavelength dependence of aerosol light absorption, nominally inverse with wavelength for soot and visible wavelengths, plays a significant role in obtaining soot loadings from remote sensing measurements (Sato et al. 2003). Soot deposition decreases snow albedo and tends towards favoring snow and ice melt (Warren and Wiscombe 1980; Grenfell et al. 1994; Hansen and Nazarenko 2004). The topic of soot in snow has its optical analogy in the contemporary instruments used to measure aerosol light absorption by filter methods. Aerosol light absorption is enhanced by roughly a factor of 2 when particles are deposited on quartz fiber filters in these instruments and by a factor of 1.4 or more on snow. The enhancement increases the signal-to-noise ratio for aerosol light-absorption measurements, although it does so at the cost of requiring an empirical calibration.

The Reno Aerosol Optics Experiment was conducted in June 2002 with the main purpose of evaluating the accuracy of aerosol light-absorption measurements. Most of the measurements were accomplished using well-characterized external mixtures of laboratory-generated ammonium sulfate and kerosene soot aerosol. A primary standard for measurement accuracy was provided by the difference of extinction and scattering measurements. Photoacoustic measurements of aerosol light absorption were in concert with the other primary standard measurement, extinction minus scattering. Details and summary results are described in Sheridan et al. (2005).

Aerosol light-absorption measurements have typically been accomplished using filter-based samplers. Here the attenuation of light across the filter is measured as a proxy for light absorption. This approach inherently overestimates the in situ aerosol light absorption because these filters are multiple scattering substrates that amplify absorption as an incidental means of improving instrument sensitivity. Various empirical approaches have been used to calibrate these instruments for aerosol light-absorption measurements. For example, the calibration model used for the particle soot absorption photometer (PSAP; Radiance Research, Inc., Seattle, WA, USA) requires additional measurements of aerosol scattering to reduce the artifact it produces on the absorption measurements (Bond et al. 1999). A three-wavelength version of the PSAP has been developed recently to measure aerosol light absorption at wavelengths (467 nm, 530 nm, and 660 nm) nearby those of the TSI nephelometer (450 nm, 550 nm, and 700 nm). Its calibration has been evaluated using data from the Reno Aerosol Optics Study (RAOS; Virkkula et al. 2005), and a new empirical filter-loading correction function was derived. This unit is not yet commercially available. One other approach for minimizing the effects of multiple scattering is to place the filter in a liquid that matches the refractive index of filter fibers (Ballach et al. 2001).

Various models of the aethalometer (Hansen et al. 1984) were recently evaluated for aerosol light-absorption measurements, and an empirical expression was developed to convert from reported values of BC concentration to aerosol light absorption (Weingartner et al. 2003). The current work, being essentially a model-based analysis of the multiple scattering problem, differs from this previous effort in that the calibration function is derived from basic theory. These workers determined an empirical function to parameterize the effects of aerosol light scattering and absorption on aethalometer response, although the use of filter attenuation in their parameterization is found to be problematic, as discussed below.

A new instrument, the multiangle absorption photometer (MAAP), was developed to measure explicitly both filter transmittance and reflectance at a wavelength of 670 nm, couple these measurements with a multiple scattering model, and thus produce a robust measure of aerosol light absorption from measurements all obtained with this single instrument (Petzold et al. 2002, 2005; Petzold and Schönlinner 2004). No ancillary measurements of aerosol scattering are needed, as the combination of transmittance and reflectance measurements sufficiently constrain the energy balance and aerosol light absorption in most circumstances. To date, a single-wavelength unit is commercially available.

The only commercially available multiwavelength aerosol light-absorption photometer is the aethalometer, Model AE-31, manufactured by Magee Scientific, Berkeley, California, USA. It operates at wavelengths of 370 nm, 470 nm, 520 nm, 590 nm, 660 nm, 880 nm, and 990 nm. The manufacturer prepares the instrument to read nominally the same BC mass concentration at all wavelengths by an assumption of inverse wavelength dependence for the relationship between light attenuation measured on the filter and BC. The question raised here is, can the instrument be calibrated as an aerosol light-absorption photometer?

Comparisons of the time series data from the photoacoustic instrument and aethalometer for white and dark aerosol limiting cases reveal insight on filter-based artifacts. A theoretical analysis of the reduced aethalometer response upon filter loading by dark aerosol is presented based on the reduction of filter multiple scattering as it darkens. This analysis leads to a model-based description of the aethalometer response to show explicitly how the BC measurements reported by the instrument could be converted to multispectral aerosol light-absorption measurements.

THE AETHALOMETER ALGORITHM FOR BC CONCENTRATION

Figure 1 illustrates the essential geometry for discussing the aethalometer algorithm (see http://www.mageesci.com/#Docs for the most current information). Let T_0 be transmission through a pristine portion of the filter, and $T(t)$ be transmission through the sample spot on the filter at time t. Transmission is formally defined as the ratio of a given detector measurement with and without the filter in place, though it will be shown that the detector measurement without the filter is not used in the algorithm.

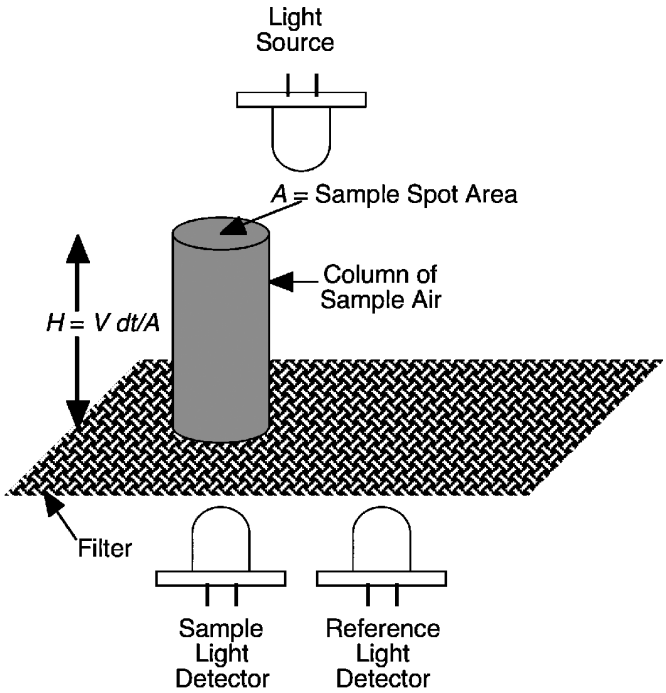

Figure 1. A column of aerosol-laden sample air of height H is deposited on the filter in time dt. Then the light source and detector are used to measure the filter transmission. Filter transmission at time t and at time $t + dt$ is used to estimate aerosol BC concentration as described in the text. A reference light detector over a pristine portion of the filter is used to measure variations in the source output.

Formal definitions are introduced here to enable the multiple scattering model development later. The algorithm introduces a variable $ATN(t)$ to represent filter attenuation through the sample spot as

$$ATN = -\ln\left[\frac{T}{T_0}\right]. \quad [1]$$

The sample light detector (reference light detector) in Figure 1 is used to measure $T(T_0)$.

Now from time t to time $t + dt$ the column of aerosol-laden sample air in Figure 1 will generally deposit particles to the filter, resulting in an increase of ATN. BC mass concentration is obtained from

$$BC(\lambda) = -\frac{d(ATN(\lambda, t))}{dt}\frac{1}{SG(\lambda)}\frac{A}{V}, \quad [2]$$

where A is the area of the sample spot to which particles are deposited and V is the volumetric flow rate, for example, given in units [lpm]. The variables that depend on the wavelength of the light source, λ, are indicated. In the words of the manufacturer, SG is the "specific attenuation cross-section for the particle black carbon deposit on this filter, using the optical components of this instrument, [m^2/g]." The manufacturer typically uses

$$SG(\lambda)\left[\frac{\mathrm{m}^2}{\mathrm{gram}}\right] = \frac{14625}{\lambda\,[\mathrm{nm}]}, \quad [3]$$

although they also mention a "Harvard" calibration using $SG = 11115/\lambda$.

The responsivity of the detectors drops out in Equation (2), as long as the detectors are linear with optical power and have constant responsivity from t to $t + dt$. The specific attenuation cross section given in Equation (3) assumes an inverse wavelength dependence for attenuation by particles deposited on the filter. At 532 nm, it is about a factor of 3 larger than theoretical values for soot-specific absorption cross sections, most likely due to the multiple scattering influence of the filter substrate on aerosol optics. The manufacturer cautions that on rare occasions the concentration of light-absorbing aerosols other than BC, or the concentration of very large BC aerosol, can invalidate the use of Equation (3).

DEVELOPMENT OF AN EMPIRICAL ALGORITHM FOR THE SCATTERING OFFSET

Measurements obtained during the Reno Aerosol Optics Experiment are used to motivate and evaluate an algorithm to convert $BC(\lambda)$ measurements to aerosol light-absorption coefficients, $B_{abs}(\lambda)$, for example, in units of Mm^{-1}, where 1 Mm = 10^6 m. Define $B_{aeth}(\lambda)$ as the attenuation coefficient resulting from putting the particles in the column of sample air onto the filter, and obtain it from the relations

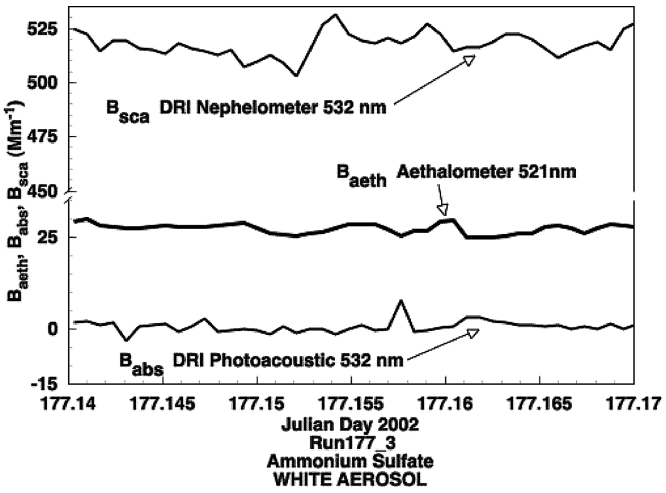

Figure 2. Aerosol optics for ammonium sulfate aerosol. Note the broken axis. The DRI photoacoustic instrument indicated no B_{abs} from these aerosol at 532 nm, though B_{aeth} is nonzero at a nearby wavelength (521 nm). B_{sca} at 532 nm is also shown. Apparently, a fraction of aerosol scattering gives the measured B_{aeth}, likely due to an increase in filter reflection (decrease in filter transmission) when aerosol is added.

$$B_{aeth}(\lambda) = SG(\lambda)\,BC(\lambda) = -\frac{d(ATN(\lambda, t))}{dt}\frac{A}{V}. \quad [4]$$

It is now demonstrated from measurement that $B_{aeth}(\lambda)$ is not equal to $B_{abs}(\lambda)$. Figure 2 shows measured aerosol optics and B_{aeth} for white ammonium sulfate aerosol, for which light absorption is very small. Some fraction of aerosol scattering gives rise to a nonzero B_{aeth}, even though $B_{abs} \approx 0$, as expected, and as measured with the photoacoustic instrument (Moosmüller et al. 1998; Arnott et al. 1999, 2000, 2003). The multiple scattering model for this case is developed in the theory section of this article. For dark aerosol with a single-scattering albedo, $\omega \approx 0.3$, Figure 3 shows considerable variation of B_{aeth} with time as the filter darkens and multiple-scatters less. The filter position was changed (automatically) when ATN changed from 1 to 0.75, and the aethalometer response was repeated.

Now towards parameterizing B_{aeth} to provide B_{abs}, the measurements in Figures 2 and 3 suggest a model similar to that used for the PSAP (Bond et al. 1999). The parameterization is

$$B_{abs}(\lambda) = \frac{B_{aeth}(\lambda) - \alpha(\lambda)B_{sca}(\lambda)}{\beta}. \quad [5]$$

The strategy is to subtract off a wavelength-dependent amount of scattering so that when white aerosols are measured, as in the data shown in Figure 2, $B_{abs} = 0$ is obtained. Once that is accomplished, the other factor, β, is determined from multiple scattering theory and the dark aerosol case as discussed below. A word of caution—the results presented here are not applicable

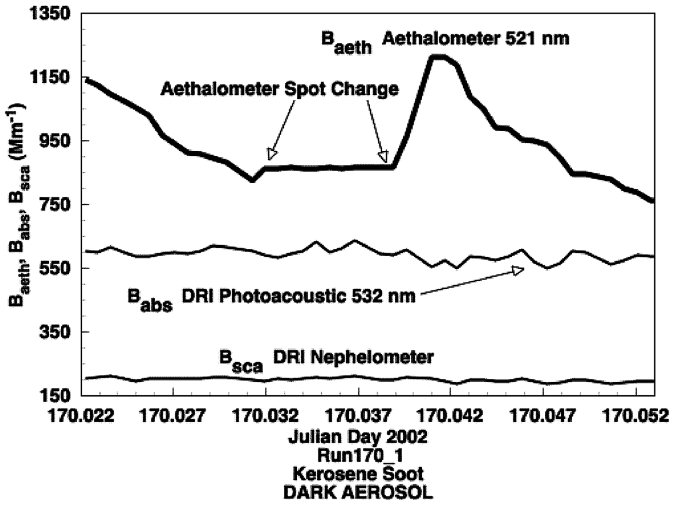

Figure 3. Aerosol optics for kerosene soot aerosol. The DRI instruments are relatively constant with time. However, B_{aeth} systematically decreases until the filter spot is changed, and then the cycle is repeated. On the average, B_{aeth} is considerably greater than B_{abs}. Apparently, the multiple scattering amplification of B_{aeth} diminishes as the filter darkens.

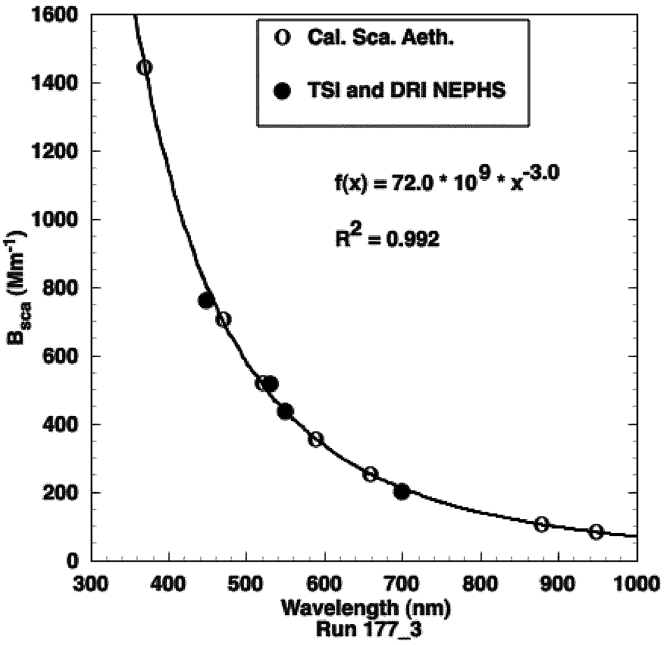

Figure 4. The O symbols are scattering measurements from ammonium sulfate aerosols made with the DRI and TSI nephelometers at 532 nm, and 450, 550, and 700 nm, respectively. The other symbols were calculated from the Ångström turbidity coefficients given in the power law relationship and are at the 7 wavelengths of the aethalometer.

to other filter media in other instruments because the multiple scattering enhancement factors vary with filter thickness and composition. However, the basic methodology may find use in other situations. The scattering-related part of Equation (5) will be explicitly calculated in the theory section. In actuality, a constant parameter β is not sufficient to bring the aethalometer and photoacoustic measurements together. Figure 3 indicates that a filter-load-dependent factor that also depends on the single-scattering albedo, ω, is necessary. The same behavior was observed from the PSAP as shown in Figure 10 of Sheridan et al. (2005).

The scattering portion of Equation (5) will be determined first. Figure 4 shows the measured spectral scattering from use of the DRI nephelometer (Varma et al. 2003) and NOAA's TSI nephelometers (Anderson et al. 1996) at wavelengths 532 nm (DRI) and 450, 550, and 700 nm (TSI) for the ammonium sulfate aerosol run averages. The time-averaged data shown in Figure 4 are from the same case presented in Figure 2. A power law fit to the measurements gives the Ångström model coefficients from use of

$$\begin{aligned} B_{sca}(\lambda) &= a\lambda^{-b}, \lambda \text{ [nm]}, \\ a &= 72.005 * 10^9, \\ b &= 2.997. \end{aligned} \quad [6]$$

The model Equation (6) is used to obtain scattering at the aethalometer wavelengths. Figure 5 shows measured values of B_{aeth} versus calculated values B_{sca} for the aethalometer wavelengths, for the average values from the time series shown in

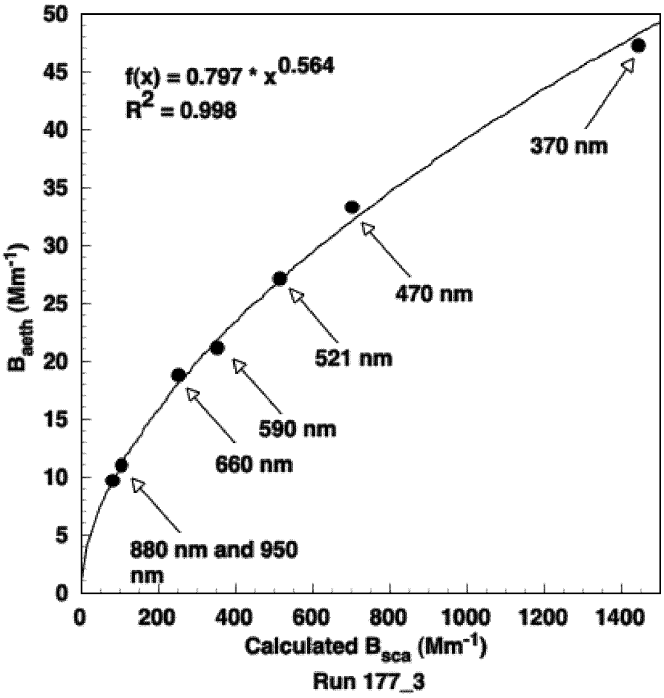

Figure 5. The calculated scattering values shown in Figure 4 are shown versus the measured B_{aeth} values from the 7-wavelength aethalometer.

part in Figure 2. A power law relationship emerges in the form

$$B_{aeth}(\lambda) = cB_{sca}^{d},\ B_{sca}(\lambda)\ [\mathrm{Mm}^{-1}],$$
$$c = 0.79732, \qquad [7]$$
$$d = 0.564,$$

where the units for scattering are given on the right. Combining the scattering portion of Equation (5) with Equations (6) and (7) gives the scattering fraction contribution to B_{aeth} as

$$\alpha(\lambda) = a^{d-1}c\lambda^{-b(d-1)},\ \lambda\ [\mathrm{nm}], \quad \text{or}$$
$$\alpha(\lambda) = 1.472 * 10^{-5}\lambda^{1.307}. \qquad [8]$$

Here α is a dimensionless quantity as long as the wavelength is given in (nm) units, and B_{sca} and B_{aeth} have common units. It appears that α dependes on particle size through the Ångström coefficients, as will be discussed in the theory section.

MULTIPLE SCATTERING CHARACTER OF AEROSOL LIGHT-ABSORPTION MEASUREMENTS BY FILTER METHODS

A two-stream model for radiative transfer in one dimension is used to simulate the response of the aethalometer. This model leans heavily on the development and insight provided in Bohren (1987). Considerable insight has already been provided in for radiative transfer by aerosol-laden filters (Clarke 1982; Gorbunov et al. 2002; Petzold et al. 2002). One goal is to build an understanding of radiative transfer by the aethalometer filter medium, particularly for a spectrum of wavelengths, and to explain why this filter media is optically dissimilar to the PSAP filter media. Then, for conservative scattering where there is no light absorption by either aerosol or the filter media, an explicit relation will be obtained for the aerosol scattering influence on aethalometer measurements (i.e., the ratio α/β in Equation (5)). Finally, a more sophisticated model that incorporates arbitrary scattering and absorbing properties of the filter and the deposited aerosol will be used to develop a filter-loading correction function for the dark aerosol case shown in Figure 3.

Figure 6 shows the measured spectral transmission for a clean filter, T_0, for aethalometer and PSAP filters. Note that PSAP transmission values and spectral variations are considerably larger than those of the aethalometer. The filter media appear similar when viewed with an optical microscope, and show transparent quartz (or borosilicate glass for the PSAP) fibers of similar sizes, and of similar packing density, in both cases backed with cellulose fibers that provide support. However, aethalometer filter media is much thicker than PSAP filter media. The relative lack of spectral variation in the Aethalometer media is a consequence of more multiple scattering than in the PSAP filter media. The tendency of each fiber is to scatter light strongly in the forward direction because of wavelength-dependent diffraction, and reflection and transmission are not observed in the light exiting the filter because light scattered by one fiber is also scattered many more times by other fibers before leaving the filter. The relative lack of spectral variation for the aethalometer filter media may be an advantage for spectral measurements of light absorption.

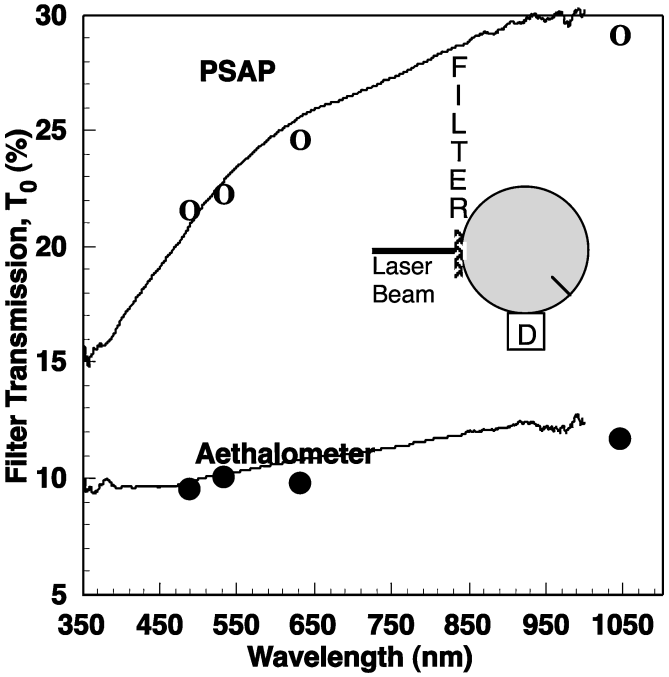

Figure 6. Measurements of the PSAP and aethalometer optical transmission at selected wavelengths accomplished using different lasers (symbols) and a spectrometer with a white light source (continuous curves). The measurement schematic is shown inset. An optical power meter is attached to an integrating sphere for the laser sources and a fiber-coupled spectrometer for the white light source. The ratio of optical power with and without the filter determines T_0.

The relevant optical parameters are now introduced. The optical depth of an aerosol-laden filter is given by

$$\tau_e = \tau_{e,f} + \tau_{e,p} = B_{ext,f}\,H + B_{ext,p}\,H, \qquad [9]$$

where subscripts p and f refer to particle and filter properties, subscript e refers to extinction, H is either filter thickness or for particles is obtained as indicated in Figure 1, and B_{ext} is the extinction coefficient. Similar definitions hold for scattering and absorption coefficients (subscripts s and a, respectively). These coefficients could be obtained by calculation from

$$B_{ext}(\lambda) = \int_0^\infty \sigma_e(\lambda, D)n(D)\,dD, \qquad [10]$$

where σ_e is the extinction cross section with dimensions of area for a particle or fiber of diameter D, and $n(D)$ is the particle or fiber number concentration distribution. However, this arduous labor will be sidestepped. The asymmetry parameter, g, for the

aerosol-laden filter is obtained from

$$g = \frac{g_f \tau_{s,f} + g_p \tau_{s,p}}{\tau_s}. \quad [11]$$

For the 1D model, g provides for the probability of forward- and backscattering (the only choices in 1D), P_{fs} and P_{bs}, as

$$P_{bs} = \frac{1-g}{2}, \quad P_{fs} = \frac{1+g}{2}, \quad [12a,b]$$

where $-1 \le g \le 1$.

Finally, the single-scatter albedo, ω, is the ratio of scattering and extinction optical depths,

$$\omega = \frac{\tau_s}{\tau_e} = \frac{\tau_e - \tau_a}{\tau_e}. \quad [13]$$

It is generally inaccurate to use Beer's law to calculate filter transmission from optical depth because multiple scattering makes it invalid.

Model for No Absorption: Conservative Scattering

All extinction is due to scattering for this model. While this is an unrealistic physical model, as all passive substances have some light absorption and a little absorption goes a long way when multiple scattering is involved, it is an instructive exercise. Filter transmission is simply given by

$$T = \frac{1}{1+\tau^*}, \quad [14]$$

where $\tau^* = \frac{1-g}{2}\tau$.

Equations (9) and (11) can be used to obtain the necessary parameters. Note that transmission cannot be used to obtain optical depth unless the asymmetry parameter is known. This case is relevant to Figure 2, where only scattering aerosol is deposited on the filter (neglecting the miniscule absorption by ammonium sulfate at these wavelengths). Equation (14) does not look at all like Beer's law.

Being careful to apply the chain rule appropriately, one can do the math indicated in Equations (1) and (4) to obtain

$$B_{aeth} = B_{sca,p}\frac{1-g_p}{2}T = B_{sca,p}P_{bs,p}T = \alpha B_{sca,p}, \quad [15]$$

where the last relation refers to the parameterization of the Aethalometer response given in Equation (5) when $B_{abs} = 0$. Equation (15) provides some justification for the choice to subtract off a fraction of aerosol scattering in the Aethalometer parameterization model of Equation (5). The physical interpretation of Equation (15) is that light reflected by the aerosol-laden filter reduces the light received by the detector in Figure 1, thereby giving a nonzero Aethalometer signal. Judging from the relative constancy of B_{aeth} in Figure 2, even for substantial $B_{sca,p}$ added to the filter over the course of the 45 min measurement run, and the expression for T in Equation (14), it must be that the g_f approaches unity and that τ_f is quite large relative to unity. Equation (15) suggests the use of a relatively low transmission filter to minimize the scattering influence, implying for example that it might be wise to use aethalometer filter media in the PSAP (see Figure 6).

The spectral response of a filter can be obtained from Equation (14) as

$$\frac{dT}{d\lambda} = -\frac{1}{(1+\tau^*)^2}\frac{d\tau^*}{d\lambda} = -T^2\frac{d\tau^*}{d\lambda}. \quad [16]$$

For strong multiple scattering $\tau^* \gg 1$, and the spectral variation of T is washed out. It is perhaps advantageous to use filter media with small T_0 to reduce the complexity due to the spectral variation of the media.

Model for Absorbing Filters and Particles

First note that the reflection and transmission from a filter loaded with aerosol throughout its depth are given by

$$R = \frac{\omega(1-g)\sinh(K\tau_e/\mu_1)/K}{\{2-\omega(1+g)\}\sinh(K\tau_e/\mu_1)/K + 2\cosh(K\tau_e/\mu_1)}, \quad [17]$$

$$T = \frac{2}{\{2-\omega(1+g)\}\sinh(K\tau_e/\mu_1)/K + 2\cosh(K\tau_e/\mu_1)}, \quad [18]$$

where

$$K \equiv [(1-\omega)(1-\omega g)]^{1/2}. \quad [19]$$

These relations can be traced to Schuster (1905) and can be obtained from the approach described in Bohren (1987). The factor μ_1 is obtained from a more vigorous theoretical development (Sagan and Pollack 1967; Liou 2002) and is typically taken to have value between unity and $1/\sqrt{3}$. This factor relates to the average behavior of diffuse light possibly traveling at oblique angles through the multiple scattering media.

The approach described in Equations (17) –(19) assumes that particles are added to the filter in a uniform manner such that the local optical properties of the filter are the similar throughout the entire filter depth. However, microscopic evidence indicates that most aerosols are deposited in roughly the first third of the filter and that the remaining filter is relatively pristine. It is also useful to consider the limiting case where aerosols are deposited on the filter surface. Figure 7 illustrates the geometry of the two-layered system with the light source above and detector below. Each layer has transmittances and reflectances obtained from use of Equations (17) and (18). Define χ as the filter thickness of layer one divided by the total filter thickness, so that the filter portion of the optical depth of layers 1 and 2 are

$$\tau_{e,f}^{(1)} = \tau_{e,f}\chi, \quad \tau_{e,f}^{(2)} = \tau_{e,f}(1-\chi). \quad [20a,b]$$

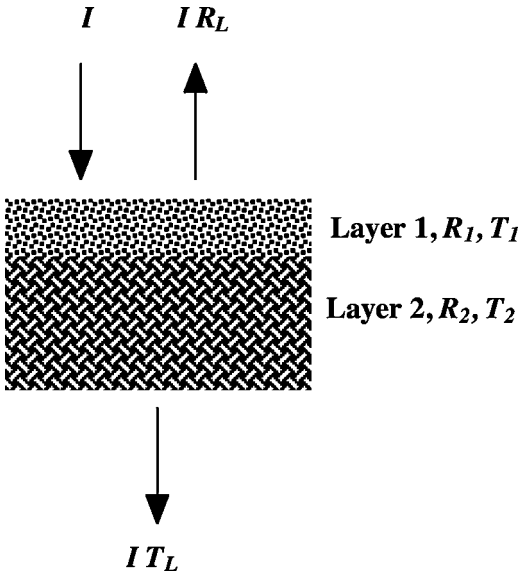

Figure 7. Two-layer model where particles are deposited on layer 1 and layer 2 remains as pristine filter media. Light from the source is signified by I, and reflection and transmission coefficients are given by R and T, respectively. This model also includes the special case of aerosols deposited on the filter surface.

The total optical depth of the layers is obtained from

$$\tau_e^{(1)} = \tau_{e,f}^{(1)} + \tau_{e,p}, \quad \tau_e^{(2)} = \tau_{e,f}^{(2)}. \qquad [21a,b]$$

The other necessary parameters such as scattering and absorption optical depths, necessary to obtain the layer reflectances and transmittances in Equations (17) and (18), can be obtained through definitions similar to Equations (20) and (21). Then the transmittance and reflectance from the two-layer system are given in (Gorbunov et al. 2002), and in the notation used in this article they are given by

$$T_{2L} = \frac{T_1 T_2}{1 - R_1 R_2}, \qquad [22]$$

and

$$R_{2L} = R_1 + \frac{R_2 T_1^2}{1 - R_1 R_2}. \qquad [23]$$

Note that the transmittance in Equation (22) is symmetric with respect to reversal of the layer subscripts, though the reflectance in Equation (23) is not symmetric. By power conservation the absorption, $A_{2L} = 1 - T_{2L} - R_{2L}$, is the fraction of optical power lost to absorption by the particle–filter system.

Figure 8 is an optical microscope photograph of a pristine portion of the aethalometer filter media. The quartz fibers shown in Figure 8 are approximately 1 μm in diameter. The milky appearance of the image comes from the multiple scattering by fibers that are out of the depth of field of the microscope objective. Figure 9 is a similar photograph of the backside of the aethalometer filter media, showing the cellulose fibers that provide support for the delicate quartz fibers. The cellulose fibers have diameters of approximately 10 μm. In principle, the multiple scattering model should include three layers: one for a surface layer where particles are deposited on the quartz fibers, one for a pristine layer of quartz fibers, and one for the cellulose

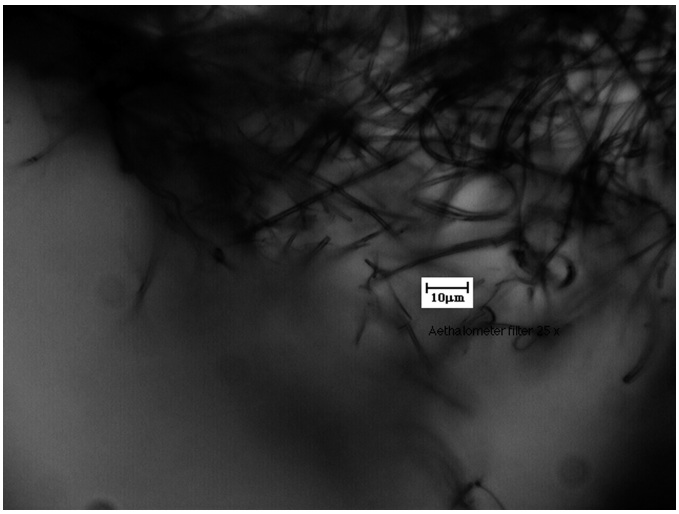

Figure 8. Optical microscope image of the quartz fibers near the surface of pristine aethalometer filter media. The milky appearance is a consequence of multiple scattering by fibers out of the depth of field of the objective. Fibers appear to be randomly oriented, and to have diameters of approximately 1 μm.

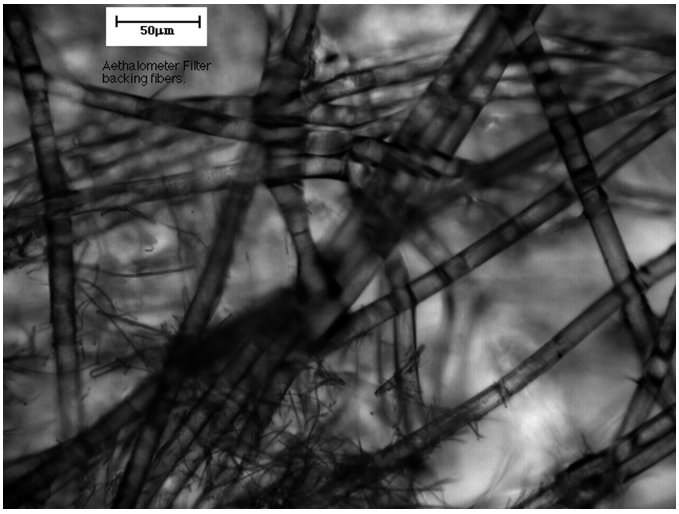

Figure 9. Optical microscope of the back side of pristine aethalometer filter media showing the cellulose backing fibers used to support the delicate quart fibers. The cellulose fibers have diameters of approximately 10 μm.

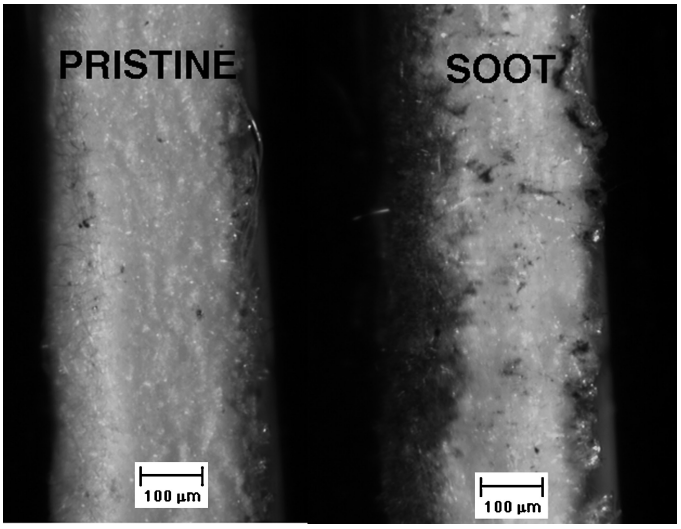

Figure 10. Optical microscope images of aethalometer filter media in cross section. The filter was sandwiched between two microscope slides. The left image shows pristine, unexposed filter (note the cellulose backing fibers near top right). The right image shows soot deposition on the media. Soot deposition is concentrated in the first third of the filter.

backing. The three-layer model has been described in Gorbunov et al. (2002), but the two-layer model will be shown to capture the essence of the multiple scattering behaviors from measurements, as given in Figures 2 and 3. Figure 10 shows a vertical slice through the middle of an aethalometer filter exposed to aerosol to illustrate the tendency for aerosols to be deposited in the first third of the filter. One would hope that all of the aerosol is deposited somewhere in the first half of the filter so that none are lost out the back.

Approximate, Practical Filter Loading Correction Function

An asymptotic, lowest-order correction function is derived as a semiempirical, practical tool to be used to convert filter transmittance measurements to aerosol light absorption. The starting point is Figure 3, where it is apparent that the simple exponential approximation embodied in the Beer's law approach of Equations (1) and (2) leads to a nonconstant time response for the aethalometer, even though aerosol delivery is stable. Beer's law is formally applicable to problems involving very low optical depths and minimal scattering. The filter cross sections in Figure 10 and the milky appearance of the filter face in Figure 8 make it very clear that optical transmission through these filters lies solidly in the multiple scattering regime.

A mathematical statement of strong multiple scattering is that the argument $(K\tau_e^{(1)}/\mu)$ in Equation (18) is of order unity or larger. Transmission through the particle-exposed portion of the filter is approximated by

$$T_1 = \frac{2\exp\left\{-K\tau_e^{(1)}/\mu_1\right\}}{\{1-\omega(1+g)/2\}/K+1}, \qquad [24]$$

where the argument of the exponential function can be expanded and expressed equivalently in either form

$$K\tau_e^{(1)}/\mu_1 = (\tau_{e,f}\chi + \tau_{e,p})^{1/2}(\tau_{a,f}\chi + \tau_{a,p})^{1/2} \times (1-g+\Omega g)^{1/2}/\mu_1 \qquad [25a]$$

or

$$K\tau_e^{(1)}/\mu_1 = (\tau_{e,f}\chi + \tau_{s,p} + \tau_{a,p})(1-\omega)^{1/2}(1-\omega g)^{1/2}/\mu_1, \qquad [25b]$$

where $\Omega = (1-\omega)$ is the coalbedo, and $\Omega \ll 1$ is likely always true because a filter change of position is initiated before total particle extinction can become comparable with filter extinction. The first form isolates the aerosol absorption optical depth, $\tau_{a,p}$, in the second square root term. The second form, Equation (25b), does the same for particle scattering in the first square root term. Multiple scattering brings in a lot of additional terms not present in the simple Beer's law approach, where one would write $T_1 = \exp(-\tau_{a,p})$. Filter extinction generally dominates the first square root term of Equation (25a), and particle absorption is seen to enter the exponential expression in Equation (24) as the square root, rather than linearly as would be expected from Beer's law.

Assuming that all of the action on filter transmission in Equation (22) due to particles being added to the filter can be attributed to the exponential portion of Equation (24), and following through on the prescription for analyzing aethalometer data as given in Equations (1) and (4),

$$B_{aeth}(\lambda) = \alpha(\lambda)\,B_{sca}(\lambda) + B_{abs}(\lambda)\frac{M(\lambda)}{\sqrt{1+\tau_{a,p}/\tau_{a,fx}}}, \qquad [26]$$

where α, M, and $\tau_{a,fx} = \chi\tau_{a,f} = \tau_{a,f}^{(1)}$ are empirical values. The filter absorption, $\tau_{a,fx}$, is the filter absorption optical depth for the filter fraction that has particles embedded in it. Notice that Equation (26) has the specific prediction that filter-loading effects, manifested in the square root term, are dependent on how deeply particles are embedded in the filter, χ. Stated as a practical algorithm used to obtain the nth measurement of aerosol light absorption after a filter change,

$$B_{abs,n} = \frac{SG\,BC_n - \alpha B_{sca,n}}{M}\sqrt{1+\frac{\left(\frac{Vdt}{A}\right)\sum_{i=1}^{n-1}B_{abs,i}}{\tau_{a,fx}}}, \qquad [27]$$

where the wavelength dependence is implied in each factor, V is the flow rate, dt is the measurement interval (typically 2 min or more for the aethalometer), and A is the filter area. The nth measurement of BC (the quantity reported by the aethalometer) is given by BC_n, and the empirical correction factor $SG(\lambda)$ is given in Equation (3). The product $(SG\,BC_n) = B_{aeth,n}$ is

Table 1
Values for use in Equation (27) to calculate light absorption from optical BC measurements

Wavelength (nm)	SG (m^2 g^{-1})	100α	M	$\tau_{a,fx}$
370	39.53	3.35	1.813	0.2736
470	31.12	4.57	2.073	0.2263
521	28.07	5.23	2.076	0.2181
590	24.79	6.16	2.104	0.1951
660	22.16	7.13	2.182	0.1777
880	16.62	10.38	2.226	0.1375
950	15.39	11.48	2.199	0.1390

These values are particularly appropriate for cases of heavy loading such as shown in Figure 3. By comparison, values of $M = 3.688$ and $\tau_{a,fx} = 0.2338$ are more appropriate for ambient measurements at 521 nm.

the raw filter-absorption coefficient, and the use of the factor *SG* simply removes the assumption made by the manufacturer about the specific absorption efficiency of BC. Equation (26) expresses that from measurement to measurement, an incremental increase of scattering aerosol on the filter causes a proportional incremental change in B_{aeth}. However, the total aerosol light absorption optical depth on the filter, $\tau_{a,p}$, reduces the net multiple scattering enhancement factor $\beta = M/(1 + \tau_{a,p}/\tau_{a,fx})^{1/2}$ of Equation (5).

Values for α, M, and $\tau_{a,fx}$ are given in Table 1. These values were derived under the following conditions. The scattering offset α is given by Equation (8) and was obtained from the ammonium sulfate "white" aerosol case in Figures 2, 4, and 5. The other coefficients were obtained from the kerosene soot case given in Figure 3 under a condition that the wavelength-dependent aerosol light absorption, when extrapolated to 532 nm with an inverse wavelength dependence on light absorption (see Sheridan et al. 2004), all give the same value as the photoacoustic measurement at 532 nm. The other condition is that the initial aethalometer values after the filter change (around time 170.042 in Figure 3) should match those at the end of the run at time 170.052, right before the next filter change. It should be noted that the light-absorption-related part of Equation (27) is generally more important to include than the scattering part when the aerosol single-scattering albedo is below 0.98.

Figure 11 shows the wavelength dependence of the parameters in M and $\tau_{a,fx}$, as well as the time-averaged spectral light absorption from the time period shown in Figure 12. Figure 12 shows that this approach to correcting for filter loading really does flatten out the strong variation of B_{aeth} observed for very dark aerosol. It should be noted that Equation (27) requires strict attention to the details of flow rate and deposition area, as the accumulated particle-associated light absorption optical depth grows in time according to these factors.

Equation (27) expresses a need to identify when the previous filter change was made by the aethalometer and to keep track of accumulated B_{abs} values. Fortunately, filter attenuation

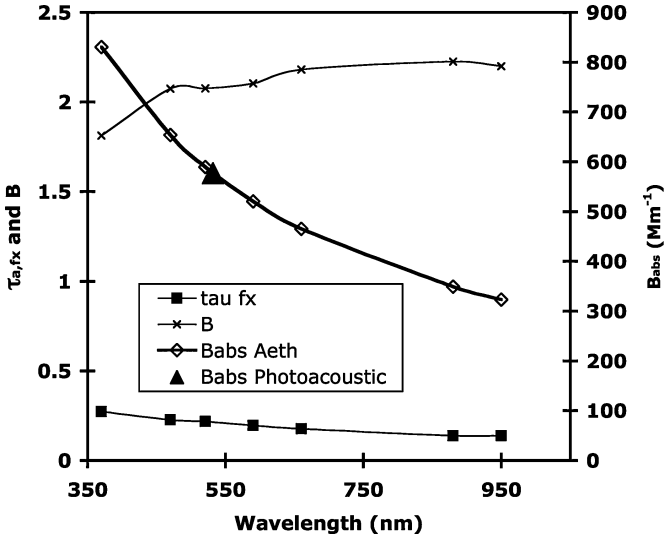

Figure 11. Wavelength dependence of the empirical coefficients $\tau_{a,fx}$ and B (left axis, square and $\times$ symbols, respectively). Averaged processed aethalometer and photoacoustic light-absorption measurements are also shown (right axis).

is recorded in the data stream from the instrument, and it increases monotonically from the time of the last filter change up to a value of approximately 75% when the next filter change is initiated. The absorption part of Equation (27) is straightforward enough that it could be included in a future revision of the instrument control software provided by the manufacturer, although it should be coupled with a scattering correction. It should be emphasized that Equation (27) applies only to the aethalometer; the filters in other instruments, such as the PSAP,

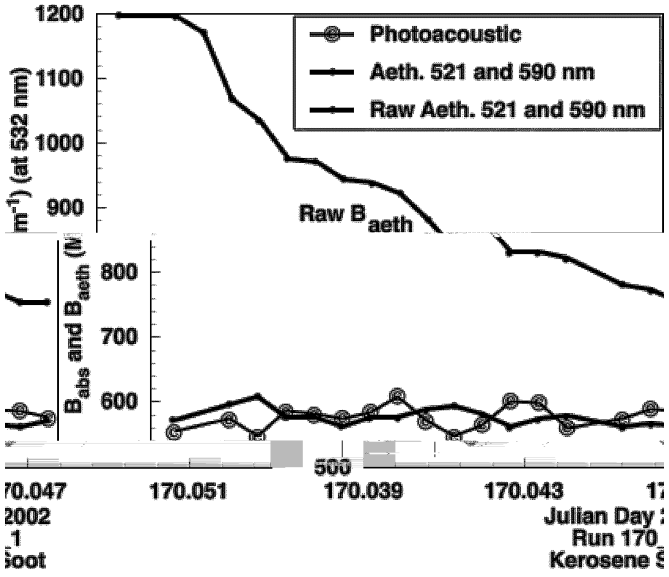

Figure 12. Raw and processed aethalometer data at 521 nm and 590 nm interpolated to 532 nm and averaged, along with the photoacoustic measurements at 532 nm as a function of time.

have different optical qualities. The approach taken in this article could help guide choice of a model-based correction function for the PSAP.

One potential snag that the user of this methodology should be aware of is that the aethalometer undergoes a filter-preconditioning cycle lasting several minutes after a tape change. The filter is exposed to sample air during this cycle. This is normally not an issue for ambient measurements, but it could be an issue when sampling from dirty sources. Another snag is that values of α were obtained from use of submicron ammonium sulfate aerosol with a specific asymmetry parameter, and they may not be applicable to drastically different aerosol such as supermicron dust. Finally, the coefficients, $\tau_{a,fx}$, will likely be different for absorbing aerosol that embed deeper or more shallow than do kerosene soot aerosol. It might be useful to include a 1 μm cutpoint impactor upstream of the Aethalometer to prevent large, nonabsorbing aerosol from clogging the filter, with attendant effects on the depth to which absorbing aerosol embed. However, this approach automatically assumes that supermicrometer particles do not absorb appreciable amounts of light. The approximation given in Equation (27) does not work for $\chi \Rightarrow 0$ because the central assumption, given in the second paragraph of this section, breaks down in this limit. One must return to the complete model in this case.

For reference, the model gives an approximate theoretical prescription for the scattering offset factor as

$$\alpha = \frac{\sqrt{\Omega_f(1-g_f)}}{\mu_1}, \qquad [28]$$

and for the multiple scattering enhancement factor

$$M = \frac{\sqrt{(1-g_f)/\Omega_f}}{2\,\mu_1}, \qquad [29]$$

where Ω_f and g_f are the coalbedo and asymmetry parameter of the filter fibers. These factors could perhaps be obtained from the detailed microphysical structure of the fibrous material, using scattering code for an infinite cylinder and a distribution of cylinder diameters centered on a nominal diameter of 1 μm. The term associated with asymmetry parameters in Equations (28) and (29) can be interpreted as the probability for backscatter by the fibrous material, as discussed below Equation (15). The term Ω_f can not be taken to zero without violating the central assumption of Equation (24).

Application to Ambient Measurements at an Urban Site

Ambient measurements of aerosol optics and chemistry were obtained from 1 January 2003 until 15 February 2003 at the Clark County air quality monitoring site on East Charleston Street, Las Vegas, NV. Las Vegas sits in a broad basin, being surrounded by mountains or hills on all sides. The site is located east of the downtown area, with winds predominantly from the west and southwest. Conditions were rather stagnant during this time period, with very few weather fronts passing through to push out the polluted air. Traffic, dust entrainment, restaurants, and residential wood burning affect the local area air quality. Figure 13a shows a scatter plot of photoacoustic measurements at 532 nm and 1047 nm made with two separate instruments. Aethalometer BC measurements at 880 nm, shown in Figure 13b, show strong correlation to photoacoustic measurements at 532 nm, with a slope of 8.84 m^2/g. Each data point is an average for the data during a particular hour of the day, taken over the 45-day time period. Such a long time average tends to smooth out the aethalometer variations seen, for example, in Figure 3.

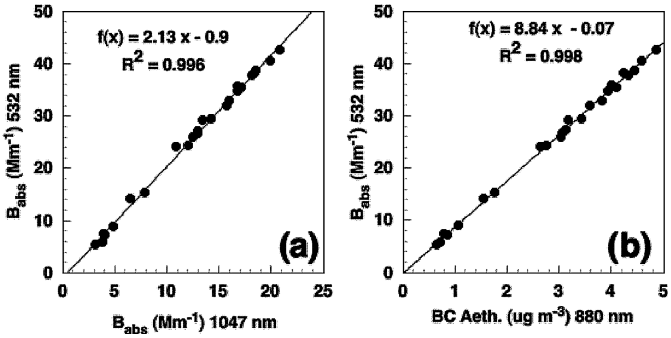

Figure 13. Scatter plots of photoacoustic measurements of (a) aerosol light absorption at 532 nm and 1047 nm, and (b) aethalometer BC at 880 nm and photoacoustic measurements at 532 nm. Each data point is an hourly average for a particular hour from the entire data set of 45 days. A broad minimum occurred in hours between 12:00 and 15:00 local, with the maximum concentrations occurring between 7:00 and 9:00. Another relative maximum occurred between the hours of 21:00 and midnight.

Average filter attenuation against the difference of photoacoustic and scaled BC measurements (using the slope in Figure 13) is shown in Figure 14. Such a long time average over many tape changes, with each data point representing a particular hourly average done 45 times over the course of the experiment, has the effect of representing the aethalometer data at an average filter attenuation. Filter attenuation is defined in Equation (1) and is reported in the data stream from the aethalometer. Figure 15 shows the same comparison, though this time for 5 min time-averaged data, further averaged into bins associated with certain ranges of aethalometer attenuation measurements. Now the trend of reduced BC measurements with increasing filter loading is apparent. The same trend in filter loading was noted in Figure 3 for laboratory-generated kerosene soot aerosol.

Aethalometer BC measurements at 521 nm were processed to light absorption values by use of Equation (27). The light-scattering values were taken from nephelometer measurements at 532 nm made with the DRI nephelometer (Varma et al. 2003). However, the coefficients M and $\tau_{a,fx}$ from the 521 nm row of Table 1 gave unsatisfactory results when comparing processed aethalometer and photoacoustic measurements. Instead, values of $M = 3.688$ and $\tau_{a,fx} = 0.2338$ were found to reduce greatly the dependence of this difference on filter attenuation. Figure 16 shows the difference of photoacoustic measurements

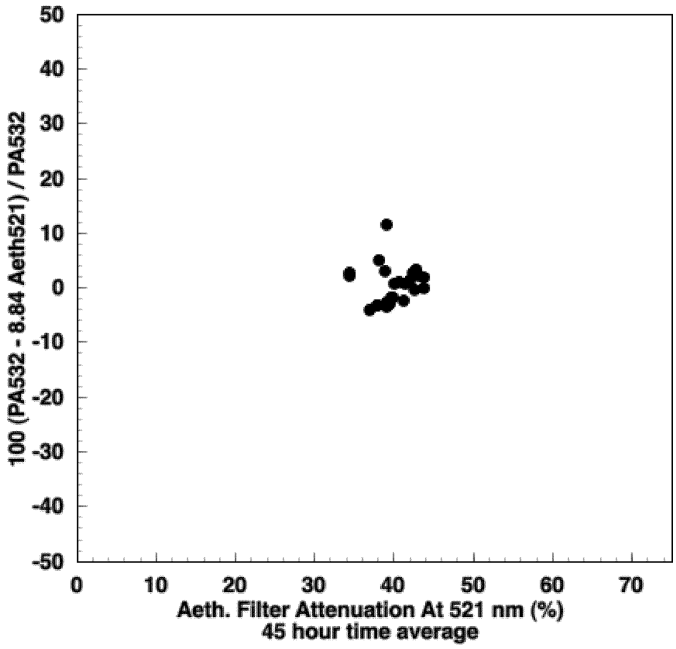

Figure 14. Scatter plot of the average aethalometer filter attenuation at 521 nm and the difference of photoacoustic and scaled BC measurements. Each point represents the hourly average for a particular hour of the day, thereby representing a 45 h average. Filter attenuation is midway between a clean filter and a fully loaded filter, whereupon a filter change is initiated. Time averaging a relatively steady source over such a long period and many tape changes brings the measurements into close agreement.

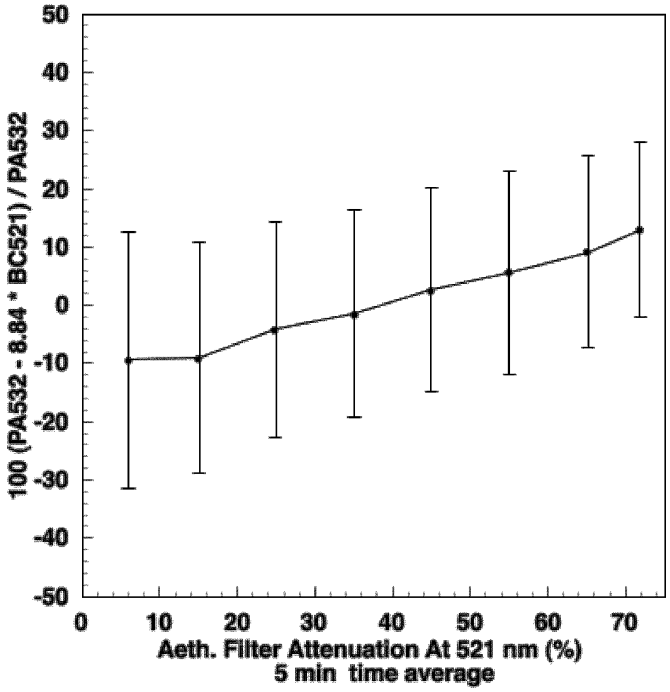

Figure 15. Same as Figure 14, except that each point represents 5 min time-averaged data placed into attenuation bins. Error bars indicate standard deviation. The trend for reduction of aethalometer BC with increasing filter attenuation is evident.

at 532 nm and processed aethalometer measurements at 521 nm (and scaled with the ratio 521/532) as a function of filter attenuation. The observation that different parameter values are needed for ambient and laboratory-generated aerosol requires further discussion.

DISCUSSION

In summary, use of the filter-loading function in Equation (27) to process the ambient (Las Vegas, NV) aethalometer measurement to light-absorption values was successful in reducing the notable effects of filter attenuation, although only by using a different set of empirical factor for M and $\tau_{a,fx}$ than those suggested from the laboratory measurements shown in Figure 3. How can this be? It is hypothesized that the effects of loading during the filter acclimatization phase after a tape change and before any optical measurements on the filter are made caused the filter to be significantly blackened before the measurements even began in Figure 3. With filter preloading before optical measurements, the multiple scattering enhancement factor, M, is already reduced by an arbitrary amount that depends on the particular situation. The effect is most notable when sampling from dirty sources as in the kerosene soot case shown in Figure 3.

Some recommendations are as follows. The aethalometer user might consider using an inline particle filter during the filter acclimatization stage after a filter change and before optical measurements ensue. The particle filter should be conditioned to ambient relative humidity (RH) and temperature well before it is used during a filter change. The reference measurements on the filter can then be taken with a pristine filter for all situations. Sample measurements are then all referenced to a pristine filter rather than to an arbitrarily loaded filter. While the aethalometer algorithm uses the difference in filter transmission between successive measurements to obtain BC concentration, the filter multiple scattering enhancement factor $\beta = M/(1 + \tau_{a,p}/\tau_{a,fx})^2$ depends on the time history since the tape change of the total aerosol absorption optical depth on the filter. It is likely that a single set of values, though different from those in Table 1, could be used if the starting point of measurement is a pristine filter. BC measurements at longer wavelengths generally have less of a range of attenuation values than those at shorter wavelengths (for the multiwavelength aethalometer) and less of a change in the multiple scattering enhancement factor; they are best for applications requiring only BC concentrations.

CONCLUSION

It has been noted by many researchers that the aethalometer values prior to a filter change are generally, but not always, lower

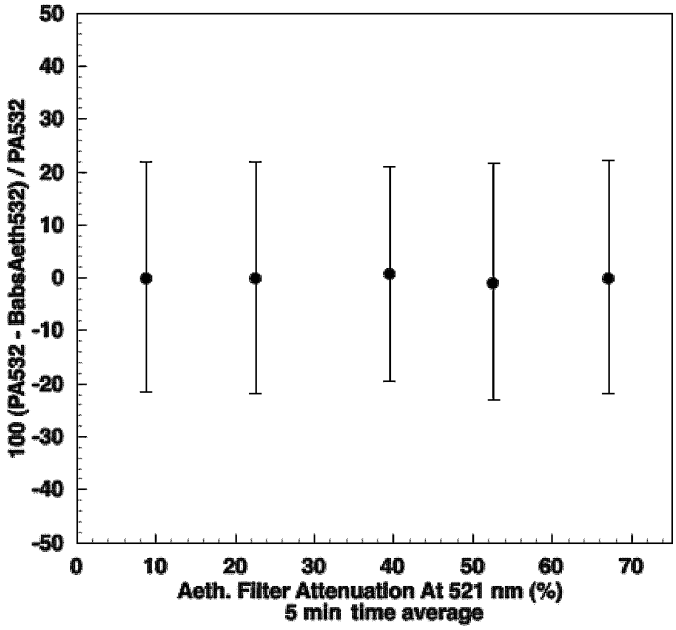

Figure 16. Average aethalometer filter attenuation at 521 nm and the difference of photoacoustic and processed aethalometer light absorption at 532 nm. Aethalometer data was processed using Equation (27), though with parameters $B = 3.688$ and $\tau_{a,fx} = 0.2338$ rather than those given in Table 1 for the 521 nm row. Aethalometer light absorption was then scaled to 532 nm by multiplying with a factor 521/532. Each point is 5 min time-averaged data placed into attenuation bins, as in Figure 15. Use of Equation (27) tends to make the difference independent of filter attenuation.

than those after a filter change. Scattering aerosol cause an incremental increase in the measured attenuation, ATN, leading eventually to an automatic filter position change in the aethalometer and a small incremental change that is accounted for as in Equation (27). The aerosol light absorption causes a reduction in the filter multiple scattering enhancement factor and is the culprit behind the noted apparent jump in aethalometer values before and after a filter change. Equation (27) offers a prescription for computing aerosol light-absorption values from measurements of BC concentration by the multi-wavelength Aethalometer. It comes about because multiple scattering strongly affects measurements of aerosol light absorption when particles are embedded in thick filter media.

The aethalometer response to laboratory and ambient aerosol was presented in this article. A loading correction function was derived based on multiple scattering theory, was applied to both aerosol types, and was found to need different coefficients in these two cases. One explanation for this lies in variable particle preloading during the filter equilibration stage after a filter change and before new measurements commence. Future work along these lines should concentrate on similar aerosol tests, although this time with explicit removal of the variable filter-preloading stage by the use of a particle filter that allows for filter equilibration with ambient RH but that does not arbitrarily blacken the filter before measurements commence.

Finally, a key prediction of the radiative transfer model for filter response is that the measurement is sensitive to how deeply the particles embed in the filter. This point is implicit in both the simple filter-loading correction function as well as in the use of the full model. Differences in the depth of particle deposition may also be related to the requirement of different empirical correction factors for ambient and laboratory-generated aerosol. Rather large particles in combination with small ones may end up sitting on the surface of the filter, whereupon the multiple scattering enhancement of particle light absorption by filter fibers is reduced in comparison with particles embedded uniformly throughout the filter. One could study this issue by using the well-known Palas Soot particle generator for small particles, kerosene soot for more "typical" soot particles, ammonium sulfate for small nonabsorbing particles, and resuspended dust for large particles that variably absorb and scatter, depending on the wavelength. This issue is particularly important for the quantification of light absorption by dust.

REFERENCES

Anderson, T. L., Covert, D. S., Marshall, S. F., Laucks, M. L., Charlson, R. J., Waggoner, A. P., Ogren, J. A., Caldow, R., Holm, R. L., Quant, F. R., Sem, G. J., Wiedensohler, A., Ahlquist, N. A., and Bates, T. S. (1996). Performance Characteristics of a High Sensitivity, Three Wavelength, Total Scatter/Backscatter Nephelometer, *J. Atmos. Oceanic Technol.* 13:967–986.

Andreae, M. O. (2001). The Dark Side of Aerosols, *Nature* 409:671–672.

Arnott, W. P., Moosmüller, H., Rogers, C. F., Jin, T., and Bruch, R. (1999). Photoacoustic Spectrometer for Measuring Light Absorption by Aerosols: Instrument Description, *Atmos. Environ.* 33:2845–2852.

Arnott, W. P., Moosmüller, H., Sheridan, P. J., Ogren, J. A., Raspet, R., Slaton, W. V., Hand, J. L., Kreidenweis, S. M., and Collett, J. L. (2003). Photoacoustic and Filter-Based Ambient Aerosol Light Absorption Measurements: Instrument Comparisons and the Role of Relative Humidity, *J. Geophys. Res.* D1: 4034.

Arnott, W. P., Moosmüller, H., and Walker, J. W. (2000). Nitrogen Dioxide and Kerosene-Flame Soot Calibration of Photoacoustic Instruments for Measurement of Light Absorption by Aerosols, *Rev. Sci. Inst.* 71(7):4545–4552.

Ballach, J., Hitzenberger, R., Schultz, E., and Jaeschke, W. (2001). Development of an Improved Optical Transmission Technique for Black Carbon (BC) Analysis, *Atmos. Environ.* 35(12):12.

Bohren, C. F. (1987). Multiple Scattering of Light and Some of Its Observable Consequences, *Am. J. Phys.* 55:524–533.

Bond, T. C., Anderson, T. L., and Campbell, D. (1999). Calibration and Intercomparison of Filter-Based Measurements of Visible Light Absorption by Aerosols, *Aerosol Sci. Technol.* 30(6):582–600.

Clarke, A. D. (1982). Integrating Sandwich: A New Method of Measurement of the Light Absorption Coefficient for Atmospheric Particles, *Appl. Opt.* 21:3011–3020.

Gorbunov, G., Hamilton, R. S., and Hitzenberger, R. (2002). Modeling Radiative Transfer by Aerosol Particles on a Filter, *Aerosol Sci. Technol.* 36(2):123–135.

Grenfell, T. C., Warren, S. G., and Mullen, P. C. (1994). Reflection of Solar Radiation by the Antarctic Snow Surface at Ultraviolet, Visible, and Near-Infrared Wavelengths, *J. Geophys. Res.* 99(D/9): 18,669.

Hansen, A. D. A., Rosen, H., and Novakov, T. (1984). The Aethalometer—An Instrument for the Real-Time Measurement of Optical Absorption by Aerosol Particles, *Sci. Total Environ.* 36:191–196.

Hansen, J. E., and Nazarenko, L. (2004). Soot Climate Forcing via Snow and Ice Albedos, *Proc. Nat. Acad. Sci. USA* 101:423–428.

Liou, K. N. (2002). *An Introduction to Atmospheric Radiation*, Academic Press, San Diego, CA.

Moosmüller, H., Arnott, W. P., Rogers, C. F., Chow, J. C., Frazier, C. A., Sherman, L. E., and Dietrich, D. L. (1998). Photoacoustic and Filter Measurements Related to Aerosol Light-Absorption During the Northern Front Range Air Quality Study (Colorado 1996/1997), *J. Geophys. Res.* 103(D21):28149–28157.

Petzold, A., Kramer, H., and Schönlinner, M. (2002). Continuous Measurement of Atmospheric Black Carbon Using a Multi-Angle Absorption Photometer, *Environ. Sci. Poll. Res.* 4:78–82.

Petzold, A., Schloesser, H., Sheridan, P. J., Arnott, W. P., Ogren, J. A., and Virkkula, A. (2005). Evaluation of Multi-Angle Absorption Photometry for Measuring Aerosol Light Absorption, *Aerosol Sci. Technol.* 39:40–51.

Petzold, A., and Schönlinner, M. (2004). Multi-Angle Absorption Photometry—A New Method for the Measurement of Aeorsol Light Absorption and Atmospheric Black Carbon, *J. Aerosol Sci.* in press.

Sagan, C., and Pollack, J. B. (1967). Anisotropic Nonconservative Scattering and the Clouds of Venus, *J. Geophys. Res.* 72(2):469–477.

Sato, M., Hansen, J., Koch, D., Lacis, A., Ruedy, R., Dubovik, O., Holben, B., Chin, M., and Novakov, T. (2003). Global Atmospheric Black Carbon Inferred from AERONET, *Proc. Nat. Acad. Sci. USA* 100(11):6.

Schuster, A. (1905). Radiation Through a Foggy Atmosphere, *Astrophys. J.* 21:1–22.

Sheridan, P. J., Arnott, W. P., Ogren, J., Anderson, B. E., Atkinson, D. B., Covert, D. S., Moosmuller, H., Petzold, A., Schmid, B., Strawa, A. W., Varma, R., and Virkkula, A. (2005). The Reno Aerosol Optics Study: Overview and Summary of Results, *Aerosol Sci. Technol.* 39:1–16.

Varma, R., Moosmuller, H., and Arnott, W. P. (2003). Toward an Ideal Integrating Nephelometer, *Opt. Lett.* 28(12):1007–1009.

Virkkula, A., Ahlquist, N. C., Covert, D. S., Arnott, W. P., Sheridan, P. J., Quinn, P. K., and Coffman, D. J. (2005). Modification, Calibration, and a Field Test of an Instrument for Measuring Light Absorption by Particles, *Aerosol Sci. Technol.* 39:68–83.

Warren, S. G., and Wiscombe, W. J. (1980). A Model for the Spectral Albedo of Snow. II: Snow Containing Atmospheric Aerosols, *J. Atmos. Sci.* 37:2734–2745.

Weingartner, E., Saathoff, H., Schnaiter, M., Streit, N., Bitnar, B., and Baltensperger, U. (2003). Absorption of Light by Soot Particles: Determination of the Absorption Coefficient by Means of Aethalometers, *J. Aerosol Sci.* 34:1445–1463.